Method for the determination of the optical properties of highly conjugated pigments

J. L. Musfeldt*

Department of Chemistry, University of Florida, Gainesville, Florida 32611

D. B. Tanner

Department of Physics, University of Florida, Gainesville, Florida 32611

A. J. Paine

Xerox Research Centre of Canada, Mississauga, Ontario, L5K 2L1, Canada

Received December 30, 1992; revised manuscript received May 4, 1993; accepted June 2, 1993

Measurements of the near-normal solid-state-pellet reflectance of five commercially available color pigments are used to calculate the frequency-dependent complex index of refraction with the Kramers–Kronig relationship. Although it is conceptually simple, the Kramers–Kronig analysis is very sensitive to the choice of extrapolation constants that describe the reflectance behavior outside the accessible frequency range, especially in the ultraviolet. We develop a method to obtain accurate optical property data in the visible region by minimizing the difference between the absorbance calculated from the refractive index and the separately measured absorption spectrum through an appropriate choice of the high-frequency extrapolation exponent. Root-mean-square differences as low as 3% can be achieved.

PACS numbers: 78.20.-e, 78.20.Dj, 78.20.Ci, 7840.Ha.

1. INTRODUCTION

Highly conjugated molecules have received considerable attention in the past several years.[1–6] Interest has focused on the strong electronic features of (π,π^*) origin in the visible region of the spectrum and the relationship of chemical structure to perceived pigment color. Owing to the intense optical absorption processes, these materials have found applications in various optical devices, as well as for coloring agents in textiles, paints, and plastics.[1,2,5]

The measurement and the manipulation of the unique absorption characteristics of dyes and pigments is one of the major thrusts of color science. In a parallel manner, there has also been a strong interest in the prediction of optical properties of these materials, especially in the various solid-state media in which they are commonly employed.[2,7] However, predictive methods for pigments have been hampered by a variety of complex problems. Whereas the optical properties of dyes are primarily due to the absorption characteristics of the isolated molecules, the color properties of pigments are due to a combination of absorption and scattering by pigment aggregates. In practice, the scattering effects are further complicated by the aggregate size distribution.[8] Thus, in order to build a more comprehensive model for pigment particle coloration properties, predictive methods must be able to forecast the scattering properties as well.

A promising model for the simulation of pigment color properties uses Mie scattering theory to predict the absorption and the angular dependence of the scattered radiation.[9–12] Such a calculation requires both the real and imaginary parts of the refractive index of the pigment particles as input parameters, in addition to an accurate knowledge of the pigment particle size distribution. As color scientists well know, the optical data are not generally available—even for common commercial pigments. Hence we sought a method of determining the frequency-dependent real and imaginary parts of the complex refractive index with an accuracy adequate for input to a Mie scattering calculation. It should be noted that although Mie scattering is derived strictly for the scattering of a plane wave by an isolated, homogeneous sphere, these constraints can be relaxed somewhat for practical use,[10] permitting the application of this theory to pigment materials. However, because the simulation of intrinsic pigment color properties with Mie scattering is a part of our long-range modeling effort (and not the main subject of this paper), these aspects will not be discussed in detail here.

In this paper we present reflectance measurements on pigment pellets, the Kramers–Kronig analysis to obtain the phase shift on reflection, and ultimately the frequency-dependent optical constants. The merit of this method is that, unlike many other techniques, it provides a framework for the estimation of both the real and imaginary parts of the complex index of refraction. Although conceptually simple, the Kramers–Kronig analysis is very sensitive to the extrapolations describing the reflectance behavior outside the commonly accessible frequency range.[13–15] This sensitivity emphasizes the important contribution of high-energy interband transitions to the total oscillator strength of conjugated dye and pigment materials. Hence we developed a method to aid in the selection of a reasonable extrapolation behavior in the interband frequency regime.

0740-3232/93/122648-10$06.00

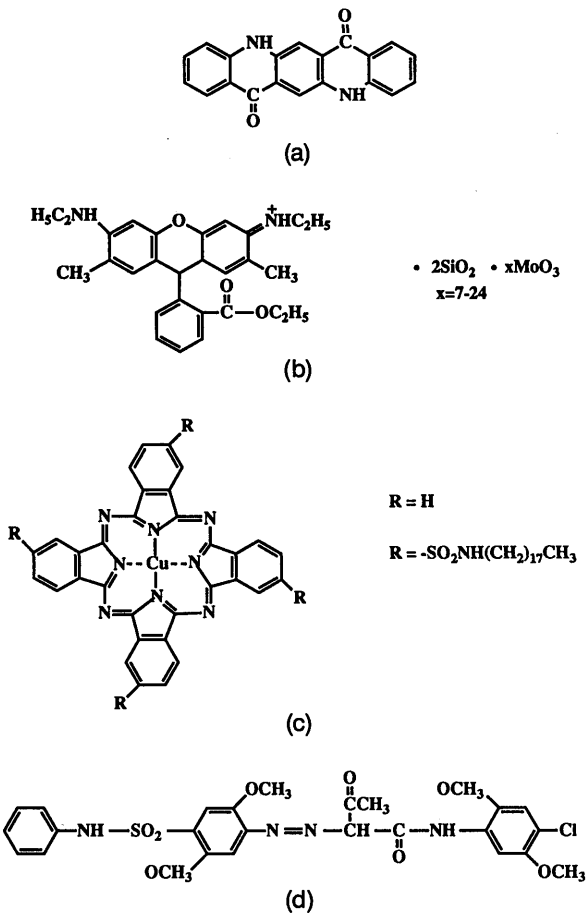

Fig. 1. Chemical structure of the pigments used in this study. The Chemical Abstracts Service registry numbers for each pigment are (a) Hostaperm Pink, 00980-26-7; (b) Fanal Pink, 75627-12-2; (c) PV Fast Blue, 00147-14-8; Neopen Blue, 39702-40-4; (d) Novoperm Yellow, 12225-18-2.

This method can be briefly summarized as follows: A Kramers–Kronig analysis of the power reflectance of the pellet samples is used to obtain a predicted bulk pigment refractive index and absorption coefficient, while transmittance measurements on the dilute pigment/toner films yield the effective absorption coefficient of these films. On account of the sensitivity of the Kramers–Kronig analysis to the choice of interband extrapolation, we use the film spectra to fix the exponent of a power-law extrapolation by closely matching the absorption coefficients from these two sets of data. Using this procedure, we were able to obtain a reliable (and Kramers–Kronig-consistent) determination of both the real and imaginary indices of refraction in the visible-frequency region. The usefulness of this method is demonstrated on a representative set of commercially available pigments.

2. EXPERIMENT

A. Pigment Samples

Five pigments were chosen as samples on which to test our method: PV Fast Blue B2G-A, Hostaperm Pink E, and Novoperm Yellow from Hoechst, and Fanal Pink D4830 and Neopen Blue NB802 from BASF. The chemical structure of each pigment is shown in Fig. 1. Note that PV Fast Blue is the well-studied copper phthalocyanine.[16–21]

For each of these materials the pigment particle size was measured to be ≈100 nm. Note that the particle size is small compared with the wavelength of light in these measurements. In addition, the loose pigment particle size is appreciably less than the bulk optical absorption depth at the wavelengths of strong absorption, such as the color band. These considerations suggest that the extinction is likely to be dominated by absorption. The extent to which the pigments are agglomerated by the pelletization procedure (described below) is discussed briefly in Section 5.

We made pellets from loose pigment powders in order to have samples suitable for reflectance studies. The powders were compressed at 0.88 GPa in an evacuated die; the pressure was maintained for 2 min and then released. Pellets were typically 1–2 mm thick and 1.6 cm in diameter. A comparison of pellet densities to bulk densities (measured with an AccuPyc 1330 instrument) indicates that the pressed pigment pellets are, on average, 93% as dense as a bulk sample. X-ray diffraction spectra before and after pelletization confirmed that the pigment crystalline polymorphs were preserved during the pressure treatment. The infrared spectra of the loose powder and the pressed pellets also displayed similar vibrational frequencies, implying that the pigment chemical and crystallographic properties were not changed by the pelletization.

B. Reflectance Measurements

Near-normal (specular) reflectance measurements were performed on the pigment pellets from 500 to 45 000 cm^{-1} at room temperature. The midinfrared spectra were collected on a Bruker 113-V Fourier-transform infrared spectrometer. Measurements at higher energy were made on a modified Perkin-Elmer grating spectrometer, whose operation has been described in detail elsewhere.[22] To improve the accuracy of the reflectance in the near ultraviolet, we coated the samples afterward with 200 nm of aluminum and measured the reflectance of the coated sample. This auxiliary measurement permitted a first-order correction to the spectra for the scattered light from the uneven pellet surface. A correction was also made for the known reflectance of aluminum. It is our experience that this procedure corrects for a majority of the surface irregularities in this frequency range.

C. Transmittance Measurements

The total transmittance spectra (specular and diffuse) were taken on xerographic solid-area images consisting of well-dispersed pigment (1–5% loading, uniform coverage) fused in a polymeric resin that was supported on a 100-μm-thick transparent plastic substrate. We call these samples pigment/toner films. These samples were measured on a Milton Roy Diano MatchScan II integrating sphere instrument by E. N. Dalal and S. Blaszak at Xerox Webster Research Center. In this mode, scattering effects were minimized by the large detector collection angle (0–90°). The specular transmittance P is collected 0–3.4° from the normal; the diffuse transmittance N is collected from the remainder of the detection angle. There is little backscatter or reflectance, so the total transmittance ($P + N$) gives a good measure of the absorptive component, independent of scattering in these films. The measured optical density was ≈1.0 at strongly

absorbing wavelengths and nearly zero at nonabsorbing wavelengths. These data were recorded over the 380–700-nm range with a 10-nm bandpass. The effective absorption coefficient is related to the measured transmittance by

$$T = \frac{(1 - R)^2 \exp(-\alpha_{\text{eff}} f h)}{1 - R^2 \exp(-2\alpha_{\text{eff}} f h)}, \tag{1}$$

where α_{eff} is the effective absorption coefficient, R is the reflectance of the pigment/toner composite system, h is the thickness, and f is the volume fraction of pigment in the sample. Neglecting the contribution of the denominator because the reflectance of the film is low, we can write the effective absorption coefficient of these films as $\alpha_{\text{eff}} = -(1/hf)\ln[T/(1 - R)^2] = -(1/C)\ln T$, where the constant C contains the sample thickness, the pigment loading in the binder, and any contribution from the binder itself to the absorption.

3. METHOD OF ANALYSIS

A. Kramers–Kronig Analysis

From a Kramers–Kronig transform of the reflectance data we calculate the index of refraction $n(\omega)$ and the extinction coefficient $\kappa(\omega)$ as functions of frequency. These properties are fundamental material characteristics, as they effectively define its optical response to light.

The Kramers–Kronig relations are based on the requirement of causality and the fact that the real and imaginary parts of a response function are always related through a dispersion relation.[13–15] For reflectance measurements the response function $r(\omega)$ is the product of an amplitude and a phase:

$$r(\omega) = E_{\text{refl}}/E_{\text{incid}} = \rho(\omega)\exp[i\Theta(\omega)], \tag{2}$$

where E is the incident or reflected electric-field vector. The measured reflectance is

$$R(\omega) = |E_{\text{refl}}/E_{\text{incid}}|^2 = \rho^2(\omega), \tag{3}$$

and the Kramers–Kronig integral relates the phase shift to the reflectance:

$$\Theta(\omega) = \frac{\omega}{\pi}\int_0^\infty \frac{\ln[R(\omega')] - \ln[R(\omega)]}{\omega^2 - \omega'^2}\mathrm{d}\omega'. \tag{4}$$

Although our data were collected over a wide frequency range (500–45 000 cm^{-1}), extrapolation beyond the frequency interval of interest is necessary, as the integral in Eq. (4) extends from zero to infinity. The details of these extrapolations and the effect on the resulting n and κ in the visible-frequency regime are the subject of Subsection 3.B.

Using

$$r(\omega) = \frac{(n - 1) + i\kappa}{(n + 1) + i\kappa}, \tag{5}$$

one can obtain the real and imaginary parts of the complex refractive index. The refractive index n is

$$n(\omega) = \frac{1 - R(\omega)}{1 + R(\omega) - 2[R(\omega)]^{1/2}\cos[\Theta(\omega)]}, \tag{6}$$

and the extinction coefficient κ is

$$\kappa(\omega) = \frac{2[R(\omega)]^{1/2}\sin[\Theta(\omega)]}{1 + R(\omega) - 2[R(\omega)]^{1/2}\cos[\Theta(\omega)]}. \tag{7}$$

The absorption coefficient α can be obtained as

$$\alpha(\omega) = 4\pi\kappa\omega, \tag{8}$$

where ω is the frequency in wave numbers (cm^{-1}). Thus, by a Kramers–Kronig analysis of reflectance data, we can obtain the optical constants of a material.

B. Method of Extrapolation

The integral in Eq. (4) can be broken into three parts:

$$\Theta(\omega) = \int_0^{\omega_{\min}} I(\omega)\mathrm{d}\omega + \int_{\omega_{\min}}^{\omega_{\max}} I(\omega)\mathrm{d}\omega + \int_{\omega_{\max}}^{\infty} I(\omega)\mathrm{d}\omega, \tag{9}$$

where $I(\omega)$ is the integrand and $\omega_{\min}$ and $\omega_{\max}$ are the minimum and maximum frequencies of available data, respectively. The middle term is evaluated numerically by trapezoidal integration.[23] The two other integrals are calculated with extrapolation procedures.

High-Frequency Extrapolation

The high-frequency extrapolation is meant to account for two distinctly different regimes: the interband region, where there is some (unknown) contribution to the optical response from interband transitions, and the higher-energy free-electron region.[13–15] It is common to model the reflectance with power laws in ω because then the third integral in Eq. (9) can be evaluated analytically by expansion in a power series.[13] In the interband region, from 45 000 to 1.0×10^6 cm^{-1}, the reflectance is modeled as

$$R(\omega) = R_f(\omega_{\max}/\omega)^E, \tag{10}$$

where R_f and $\omega_{\max}$ are the reflectance and the frequency of the last measured data point, respectively, and E is an adjustable exponent, typically taking on a value between zero and four. Above $\omega_A = 1.0 \times 10^6$ cm^{-1}, free-electron behavior

$$R(\omega) = R_{f'}(\omega_A/\omega)^4 \tag{11}$$

was assumed.[13–15] Here $R_{f'}$ is defined as

$$R_{f'} = R_f(\omega_{\max}/\omega_A)^E, \tag{12}$$

and ω_A is the frequency at which free-electron behavior is obeyed. Hence the high-frequency extrapolation of the Kramers–Kronig analysis has two adjustable parameters: E, the interband exponent, and ω_A, the frequency of free-electron behavior. A reasonable choice of these two parameters is critical to the success of this method.

Figure 2 displays the reflectance of a typical pigment sample in which several high-frequency (interband) extrapolations in Eq. (10) are shown ($E = 0, 1, 2, 4$). When the exponent is large, the cutoff is very steep and significantly less area is included in the calculation of the phase integral. This choice results in the assignment of most of the oscillator strength to energies below ω_A. Con-

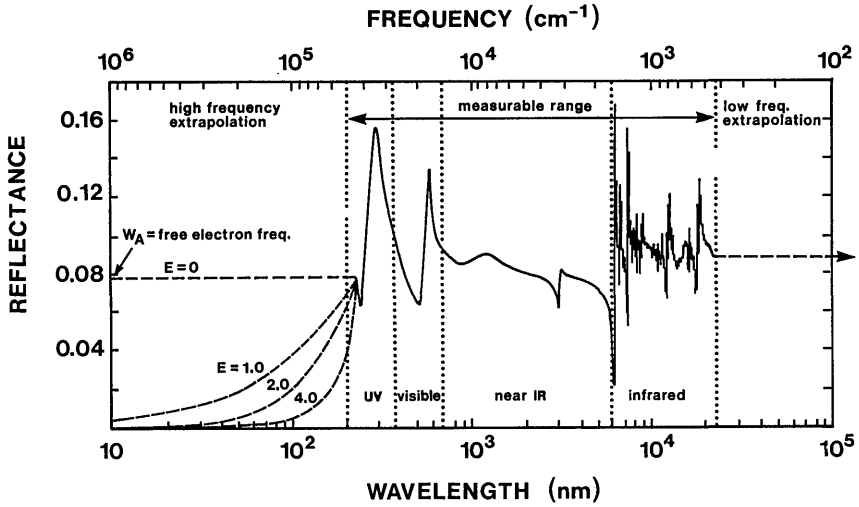

Fig. 2. Typical reflectance spectrum at room temperature. The solid curve corresponds to measured data, and the dashed curves represent various extrapolations at high and low frequencies.

versely, if the exponent is artificially low, a significant portion of the total oscillator strength may be moved to energies far greater than that of the color band.

It is expected that highly conjugated materials should have intense absorptions in the ultraviolet and beyond, and thus a significant amount of spectral weight at high frequency. The difficulty lies in determining *how much* oscillator strength lies above ω_A. Hence we have developed two criteria for the optimal choice of E in these materials. In the first the exponent E is chosen to minimize the difference between the absorption coefficient as calculated from the Kramers–Kronig analysis of reflectance and the effective absorption coefficient as inferred from the specular and diffuse transmittance measurements $(P + N)$ of the pigments in the binder. As an alternative criterion one could choose to minimize the difference between the position of the minimum in the Kramers–Kronig-determined $\alpha(\omega)$ on the high-energy side of the color band and the corresponding minimum in the $\alpha_{\text{eff}}(\omega)$ spectrum of the pigment in the toner with the necessary restriction that the calculated phase in Eq. (4) be positive. The motivation for considering this second criterion is that this minimum is strongly affected by the extrapolation, whereas the location of the color-band maximum is weakly dependent on the extrapolation. However, the first criterion gave the more reliable color property results overall, hence that method and the corresponding results will be presented here.

Low-Frequency Extrapolation

The method of extrapolation at low energy in Eq. (4) must also be addressed. For nonconducting materials it is common to approximate $R(\omega)$ as a constant to zero frequency[13–15] (Fig. 2). To test the applicability of this approximation for pigment and dye materials, we measured the infrared reflectance and included these data in the calculation of the phase integral. The additional data had little effect on the resulting optical constants in the visible-frequency range because there are no major electronic transitions at low energy. Thus we conclude that, for nonconducting samples such as conjugated dyes and pigments, the low-frequency reflectance (below the optical absorption threshold) can be assumed constant, with negligible error to the optical constants in the visible region.

C. Validity of the Dispersion Relations

In this subsection it is our goal to motivate the use of the Kramers–Kronig dispersion relations to analyze the power reflectance of our bulk pigment samples and to obtain the frequency-dependent response functions. It is clear that with a pellet composed of compressed pigment powder we can expect to measure only average optical properties, not the principal components of the dielectric tensor, as might be obtained from single-crystal samples. However, for many applications involving pigment or dye materials the molecules are in a random orientation, so that a polycrystalline average is appropriate. (This is the case with dilute pigment/toner samples.) Consequently, data obtained from such a technique are likely to be extremely useful for understanding the color properties of pigments in a wide variety of applications.

Because the extinction is the sum of both absorption and scattering effects,[10,12] the amount of internal (diffuse) scattering in these bulk pellet samples is an important concern. There is a large volume of literature on this subject that suggests that an explicit inclusion of scattering effects might be important for our analysis.[11,12] However, we believe that diffuse scattering is small in these samples for several reasons. First, in the cases discussed here the apparent density of the pigment pellet is very close (93% on average) to the bulk (crystal) density. In the high-density limit diffuse scattering should be minimal because the number of scattering centers (the voids) is small.[24] Second, the pigment particle size (and thus, one expects, the size of the voids) is small compared with the wavelength. Finally, in the highly absorbing regions, such as in the highly absorbing or relaxational regimes near the color band, the penetration depth is small because of strong damping inside the sample. Consequently, internal inhomogeneity is less of a concern at these energies. In any event the success of the Kramers–Kronig analysis, as shown below, seems to justify our neglect of bulk scattering in the samples used for the reflectance spectra.

D. Least-Squares Optimization

We used a nonlinear least-squares fitting procedure to optimize the choice of high-frequency extrapolation parameters. The objective of this procedure was to minimize the difference between the absorption spectra calculated from the Kramers–Kronig analysis of pigment pellet reflectance and that measured in a dilute suspension of pigment in resin by appropriate adjustment of the Kramers–Kronig high-frequency extrapolation parameters.[25] In principle, one can manipulate both the exponent E and the free-electron value ω_A simultaneously to produce the best fit. However, because ω_A is far from the region of interest, we selected E as the optimization variable of choice and fixed ω_A at 1×10^6 cm^{-1} (124 eV).

The optimum value of E is the one that minimizes the least-squares difference (rms error) between the observed spectra and the computed absorption coefficient $\alpha(\omega)$ according to the following procedure: For each value of E we

(1) Perform the Kramers–Kronig analysis, calculating the phase from Eq. (4) and obtaining the complex refractive index $n(\omega) + i\kappa(\omega)$.[23]

(2) Convolve $n(\omega)$ and $\kappa(\omega)$ with a 10-nm bandpass to obtain $n(\lambda)$ and $\kappa(\lambda)$ corresponding to the visible-range spectra (380–700 nm at 10-nm increments).

(3) Compute the absorption coefficient α according to Eq. (8).

(4) Find the scaling constant C, which relates α to the observed thin-film transmission $T_{obs}(\lambda) = I/I_0$ (corrected for the 6% reflectance of the xerographic solid-area image samples), such that $-\ln[T_{obs}(\lambda)] = C\alpha(\lambda)$, where C is an adjustable coefficient containing the thickness h and the loading of the pigment in the binder, f, for the thin-film samples. This adjustment is readily accomplished by least-squares methods, which gives an error estimate for C, r^2, and a frequency-averaged rms fitting error,[26] the equation for which is

$$\text{rms} = 100\% \times \frac{\left\{\sum_{\lambda}[C\alpha(\lambda, E)] + \ln[T_{obs}(\lambda)]^2\right\}^{1/2}}{-\ln[T_{obs}(\min)]}. \quad (13)$$

The fitting error was scaled to the extreme value of the absorption coefficient so that the results are presented as a percentage of the maximum in $\alpha(\lambda)$.

(5) Choose the exponent E and the scaling factor C such that the rms error between the two spectra is a minimum. Our method uses a well-known least-squares minimization procedure.[26]

To summarize, the Kramers–Kronig analysis of the power reflectance of the pellet samples leads to a predicted bulk pigment refractive index and absorption coefficient, whereas the transmittance measurements on the dilute pigment/toner films yield an effective absorption coefficient. Owing to the sensitivity of the Kramers–Kronig analysis to the choice of interband exponent E, the film spectra are used to determine the exponent in the iterative manner described above. This adjustment is made in order to account properly for the missing oscillator strength above the highest measurement frequency. Using this procedure, we are able to obtain a reliable (and Kramers–Kronig-consistent) determination of both the real and the imaginary index of refraction in the visible-frequency region.

4. RESULTS

A. Reflectance Measurements

The solid-state reflectance spectra of the five pigments used in this study are shown in Fig. 3. The spectra are dominated by several strong electronic absorption bands in the visible and near-ultraviolet frequency region originating from (π, π^*) transitions, features that are similar in character to the spectra of other highly conjugated materials.[4,6,16,27]

The visible spectra of most highly conjugated pigments and dyes consist of a single main absorption of (π, π^*) origin; this strong excitation is often referred to as the color band. The wavelength, the width, the shape, and the intensity of the color band are the primary factors in determining the optical properties of the pigment.[28] In many chemical systems a shoulder is observed on the high-energy side of the color band; it is attributed to a vibrational feature of the first excited electronic state.[4,6] The magenta and blue pigments in this study clearly display this feature. For porphyrin-based materials the color band and its higher-energy shoulder are referred to as Q_α and Q_β bands, respectively.[29]

Several additional electronic features of (π, π^*) origin are observed in the near ultraviolet. Numerous spectral studies have shown that the exact position, shape, and intensity of these bands are extremely sensitive to the

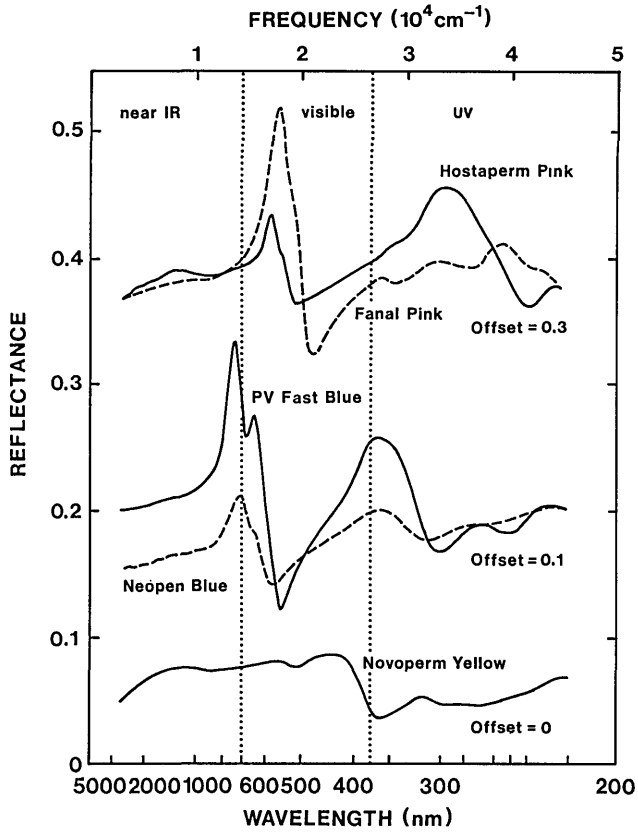

Fig. 3. Room-temperature reflectance of pure pigment pellets from 5000 to 200 nm.

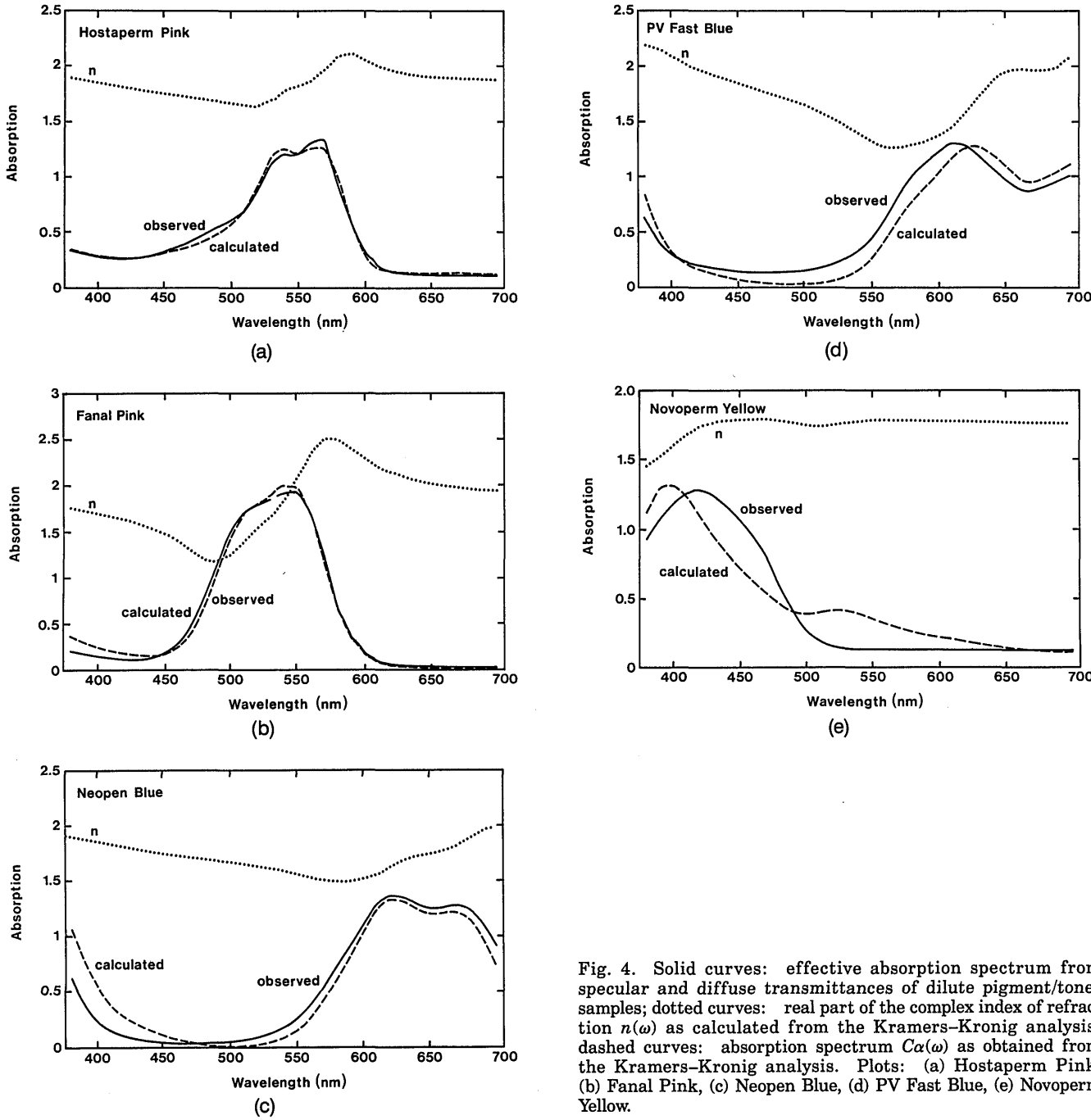

Fig. 4. Solid curves: effective absorption spectrum from specular and diffuse transmittances of dilute pigment/toner samples; dotted curves: real part of the complex index of refraction $n(\omega)$ as calculated from the Kramers–Kronig analysis; dashed curves: absorption spectrum $C\alpha(\omega)$ as obtained from the Kramers–Kronig analysis. Plots: (a) Hostaperm Pink, (b) Fanal Pink, (c) Neopen Blue, (d) PV Fast Blue, (e) Novoperm Yellow.

chemical structure of the pigment molecule.[4,6,16,27] Our measurements also support this conclusion, as evidenced by the different electronic spectra of the various pigments presented in Fig. 3. The spectral excitations in the solid state are also much broader than those reported for pigment materials in solution or in the gas phase.[6,16] In our materials the broadening is most evident above 25 000 cm^{-1} and is probably due to interactions among adjacent molecules and the broadening effects inherent in the solid state, where electronic overlap between molecules may lead to band formation.[17]

The optimal set of optical constants for the pigments is displayed in the various plots of Fig. 4. In each plot $n(\omega)$ displays the usual dispersive behavior expected at each absorption band. Extrapolation of $n(\omega)$ to zero frequency also provides an estimate of the refractive index of each pigment (Table 1). The frequency-dependent absorption coefficient in Fig. 4 has been calculated directly from $\kappa(\omega)$ through Eq. (8), permitting easy comparison with the observed pigment absorption in the binder. As we discussed

Table 1. Zero-Frequency Refractive Indices

Pigment	n
Hostaperm Pink	1.83
Fanal Pink	1.77
Neopen Blue	1.70
PV Fast Blue	1.91
Novoperm Yellow	1.74

Table 2. Color-Band Center Frequencies and Absorption Maxima in $\kappa(\omega)$ from Reflectance Measurements on Pigment Pellets

Pigment	ω Color Band (cm^{-1})	ω Sideband (cm^{-1})	α Color Band (10^5 cm^{-1})	α Sideband (10^5 cm^{-1})
Hostaperm Pink	17696	18640	0.90	0.88
Fanal Pink	18383	19480	2.38	2.06
Neopen Blue	14955	16040	0.67	0.71
PV Fast Blue	14120	16040	1.69	1.88
Novoperm Yellow	25285		1.30	

in Subsection 3.C, this calculation assumes minimal scattering in the bulk samples.

The center frequencies and the absorption coefficients of the major excitations in the visible-frequency range are presented in Table 2. The absorption coefficients of the color-band maxima are of the order of 10^5 cm^{-1}, which is common among pigments and dyes. It should be noted that, since the molar volume of the Neopen Blue is approximately 4.6 times that of PV Fast Blue, the Neopen Blue is actually a stronger absorber than the PV Fast Blue on a per phthalocyanine-center basis. Thus the full absorptive character of the Neopen Blue pigment is not readily apparent from the value in Table 2. The electron-withdrawing nature of the sulfonamide side chain is presumably responsible for the slight blue shift of the Neopen Blue color band compared with that of PV Fast Blue.

B. Effect of Interband Extrapolation

Figure 5 displays the effect of the interband extrapolation on the frequency-averaged rms error of the predicted $\alpha(\omega)$ compared with the actual spectra of the pigment in the binder. The minima are clear and well defined for all the samples except the yellow pigment. The best E values for the five pigments fall in the range 0.5–1.5 with no apparent pattern. We conclude, as might be expected, that these highly conjugated pigments have a significant fraction of their oscillator strength in the ultraviolet and beyond. Figure 5 clearly shows that, unless the interband oscillator strength is properly accounted for, the high-frequency extrapolation represents a large source of error in the application of the Kramers–Kronig method to these materials.

In three cases (Novoperm Yellow, Hostaperm Pink, and PV Fast Blue) the minimum fitting error was obtained with all the phase angles positive (in the solid curve portion of Fig. 5). However, in the cases of Fanal Pink and Neopen Blue the optimum value of E from the least-squares fitting process produces some regions of negative phase in the visible region. Because negative phase is physically unreasonable, our selected value of E includes the constraint of positive phase over the 380–700-nm interval. This constraint shifted the selected E upward slightly for Fanal Pink and Neopen Blue, giving the values indicated by the solid dots in Fig. 5. These values are reasonably close to the global minimum and can be taken as an indication of the size of the error bars in this analysis.

The results of our optimizations are summarized in Table 3. The predicted absorption spectra (as obtained from a Kramers–Kronig analysis of the reflectance) agree with the experimental spectra (obtained from transmittance measurements of thin films), with rms differences of 3–15%. The magenta pigments were the best, with only a 3% difference, whereas the yellow pigment was by far the worst. Another parameter of interest is CIELAB ΔE, which is defined as the square root of the sum of the square of the differences between the calculated and the observed a^*, b^*, and L^*, where a^* and b^* define the hue angle and L^* defines the chroma.[30] When ΔE is less than ≈ 3, color differences are imperceptible. Values for CIELAB ΔE, describing the difference between color properties predicted by the observed pigment/toner data and those calculated with the $n(\omega)$ and the $\kappa(\omega)$ obtained by a Kramers–Kronig analysis of the power reflectance, are shown in the fourth column of Table 3. These data show excellent agreement in two cases, with less good but acceptable agreement in two other cases. The final column in Table 3 gives the product of the volume fraction pigment in the toner layer, f, and the path length h. This product would correspond to the value of the scaling constant C *if* the pigments were molecularly dispersed and there were no effects that were due to particularity. Three of the pigments—Hostaperm Pink, Neopen Blue, and PV Fast Blue—seem to be in this category. The two other pigments have computed C values that are approxi-

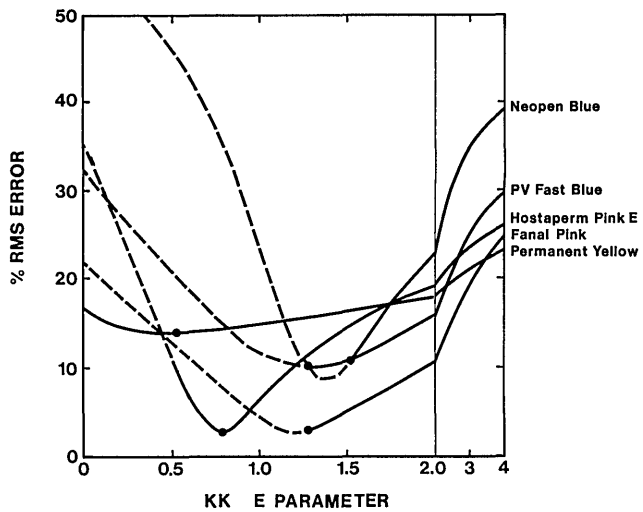

Fig. 5. Dependence of the frequency-averaged fitting error on the Kramers–Kronig (KK) extrapolation exponent for the five pigments investigated. Note the scale change for $E = 2$ to 4. The solid curves correspond to positive phase angle Θ over the 380–700-nm range, while the dashed curves correspond to at least one negative Θ value. The solid dots indicate the selected value of the interband extrapolation parameter that minimizes the least-squares difference between the computed absorption coefficient α and the observed toner film transmission while retaining positive Θ in the visible range.

Table 3. Summary of Results from Fitting Procedure

Pigment	Optimal Exponent	rms (%)	CIELAB ΔE	r^2	C (nm)	Actual fh (nm)
Hostaperm Pink	0.79	2.6	2.7	0.9969	330 ± 11	307
Fanal Pink	1.28	3.3	1.2	0.9949	197 ± 6	294
Neopen Blue	1.52	11.0	19.8	0.9614	447 ± 251	430
PV Fast Blue	1.29	10.1	18.4	0.9672	157 ± 26	148
Novoperm Yellow	0.53	14.1	35.3	0.9176	242 ± 164	351

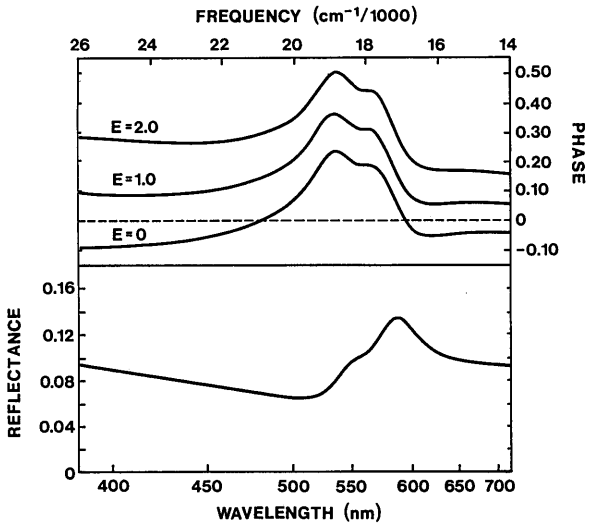

Fig. 6. Phase angle of Hostaperm Pink, $\Theta(\omega)$, as calculated from the Kramers–Kronig analysis with different interband extrapolations.

mately a third less than the actual value of fh, indicating that perhaps some of the pigment is aggregated and thus not so highly absorbing as it would be if the pigment were completely dispersed.

Figure 6 illustrates how variations in the interband extrapolation exponent are manifested in the optical spectra of Hostaperm Pink. An underestimation of the oscillator strength at high energy results in a reduced contrast between the color-band maxima and the baseline (the chroma). Overestimation of E also distorts the predicted color properties as well because the position of the color band is shifted slightly to the red as the oscillator strength of the color band is pushed to lower energy. Conversely, a too large value of the oscillator strength at high energy (a too small value of E) results in a negative phase throughout most of the frequency range of interest.

5. DISCUSSION

In the following subsections we briefly discuss the particulars of each pigment in reference to their spectra appearing in the various plots of Fig. 4, the data in Table 3, and the fitting process in general. For these samples the real part of the refractive index, n, is greater than the imaginary part κ at all the wavelengths considered here, and both optical constants display strong dispersive behavior at energies near the color band. This strong dispersion is likely to prevent applications of these materials based on index matching because of the inherent difficulty of obtaining such a match. The good agreement between the two sets of data also indicates that the extinction of the pigment samples is dominated by absorption, although rms deviations are between 3% and 15%. Several examples are presented below to demonstrate the use of this technique on a wide range of materials. Our goal is not only to highlight the obvious successes of this method but to illustrate the difficult cases as well.

A. Hostaperm Pink

The observed and calculated spectra of Hostaperm Pink are displayed in Fig. 4(a). This pigment gave the best fit of the effective absorption spectrum (as obtained from the pigment/toner films) to the Kramers–Kronig-determined absorption coefficient α, with rms error less than 3% and a very low CIELAB ΔE. The Kramers–Kronig calculations seem to generate a slight mismatch in the relative intensity near 550 nm and a hint of an additional absorption at 660 nm. On the whole, the agreement is quite good, demonstrating the validity of our interband exponent optimization procedure.

B. Fanal Pink

A Kramers–Kronig analysis of the reflectance spectrum of this material also gave an excellent fit of $\alpha(\omega)$ to the effective absorption spectrum of the pigment suspended in toner resin [Fig. 4(b)] and the lowest CIELAB ΔE value (Table 3). Some deviations between the two spectra occur in the 380–500-nm range, where scattering effects that are due to the particulate nature of the pigment would be expected to become more important. That C is significantly less than fh is another indication of the onset of particulate effects. The shape of the frequency-dependent absorption coefficient in the 380–500-nm range may also affect the overall quality of the fit. The color band in Fanal Pink is followed by a sharp, deep minimum centered at 450 nm, whereas the color band in Hostaperm Pink is broader and shallower. Since the absorption data for the pigment in the binder were obtained with a 10-nm bandpass, we are likely to obtain a better fit for broadened features, such as those in the Hostaperm Pink spectrum. On the whole, however, the results for the Fanal Pink pigment are very satisfactory.

C. Neopen Blue

The spectra of the Neopen Blue pigment are shown in Fig. 4(c). For this sample the fit error is approximately three times larger than it was for the two magenta pigments. Examination of Fig. 4(c) shows that the major difference again appears in the 380–500-nm region of the spectrum, where the pellet reflectance datum predicts greater absorption than is observed in the thin pigment/toner films. This deviation could result from scattering losses resulting from pellet features smaller than the 200-nm aluminum overcoat. Such a deviation may also result

from small inadequacies in the Kramers–Kronig extrapolation assumption, as the highly absorbing and relaxation regimes in this material are closer to the missing vacuum-ultraviolet data and so are more strongly affected by the extrapolation. Despite these shortcomings the Kramers–Kronig analysis reproduces the shape and the intensity of the color band (600–700-nm feature) very well.

D. PV Fast Blue

The spectra of PV Fast Blue (copper phthalocyanine) are displayed in Fig. 4(d). The optical properties of this material have enjoyed special attention from both the experimental[16–18] and theoretical[19–21] perspectives. The color-band features, as well as the higher-energy spectral characteristics [not shown in Fig. 4(d)], are in overall reasonable agreement with previous measurements, although the features in the optical spectra of copper phthalocyanine are slightly red shifted and broadened compared with results reported by Edwards and Gouterman[16] and others.[17,18] This band is also red shifted compared with the characteristic color-band position (670 nm) in other phthalocyanine-based materials with D_{4h} symmetry.[6] The inclusion of filler or extender in these commercial pigment samples is a possible explanation for this difference.

Although the magnitude of the fit error for this pigment is comparable with that of the Neopen Blue sample, the type of discrepancy is different and potentially more serious for color calculations of a predictive nature. As Fig. 4(d) shows, the computed absorption spectrum is red shifted from the observed spectrum of the pigment in the binder by 10–20 nm. Perhaps the denser packing in the pigment pellet introduces slight modifications to the electronic spectrum that red shift the band position slightly from its position in the binder. However, it is more likely that this difference reflects the combination of measurement difficulties (both in the pellet form and in the binder) and the limitations of the Kramers–Kronig method for this material.

E. Novoperm Yellow

The spectrum of Novoperm Yellow [Fig. 4(e)] was the most difficult to analyze and is significantly different from the four other conjugated pigments in this study. Rather than a strong color band with good contrast from a near-zero baseline absorption, as found in the dilute transmittance studies, the Kramers–Kronig analysis yields several broad and overlapped features in the visible energy region. Although the gross features of the observed absorption spectrum are captured in the spectrum computed by the Kramers–Kronig procedure, the Kramers–Kronig analysis suggests a secondary absorption near 530 nm in the bulk pigment that is absent in the effective absorption spectrum of the dilute pigment/toner film. In addition, the main absorption peak in the optical regime is blue shifted by 20 nm compared with what is observed in the dilute pigment/toner samples.

At the present time we have only tentative explanations for the discrepancy between optical constants as obtained by a Kramers–Kronig analysis of bulk pigment reflection and the direct absorption measurements on dilute pigment/toner films for Novoperm Yellow. One possibility is that there may be a preferential orientation in the pressed pellets in this anisotropic material.[31] In this case our reflectance measurements may have oversampled one axis, perhaps one with charge-transfer character, thereby producing the deviation from the (randomly oriented) pigment/toner absorption that we observe in Fig. 4(e). It is also possible that the feature at 530 nm may be a solid-state (rather than isolated molecule) effect, with the flexible nature of the pigment molecule providing an opportunity for adjacent molecules to be in close proximity and thus for charge transfer between intermolecular quinoid rings.

The deviation between the position color bands of the computed and observed absorption spectra also points out the inherent difficulties of the Kramers–Kronig method for materials that absorb in the violet: features nearer to the high-frequency limit of the measurement are not so reliable as those away from it. This is the most likely explanation for the observed discrepancy in the color-band feature. The spectra shown in Fig. 4(e) illustrate what is, in our experience, a worst-case scenario. This result should serve as a warning about the limitations of the Kramers–Kronig technique—the results need to be interpreted with care.

6. CONCLUSION

We have presented a method based on the Kramers–Kronig relationship to automate the determination of reliable optical constants in the neighborhood of the color band in highly conjugated pigments and dyes. The choice of the high-frequency exponent is the key to a meaningful analysis of the optical properties of these pigments because of the large spectral weight of the interband transitions in the ultraviolet-frequency range. We demonstrate the effect of various exponents on the character of the color-band absorption and develop criteria for the optimal choice of the high-frequency interband exponent in these highly conjugated materials.

The major advantage of a dispersion-based method, such as that outlined here, is that it provides a framework in which the real and imaginary parts of the complex index of refraction are obtained in a self-consistent manner. It is also conceptually simple and readily applicable to common use. Consequently, this technique is likely to see wide application in the field of color science.

The capabilities of our optimization method in calculating $n(\omega)$ and $\kappa(\omega)$ were demonstrated on a representative set of five commercially available pigments. Our future research centers on the use of real and imaginary refractive indices obtained in this manner as input to Mie scattering calculations, with the ultimate goal of modeling the color properties of pigment/toner systems.

ACKNOWLEDGMENTS

The authors thank E. N. Dalal, S. Jeyadev, and I. Morrison of Xerox Webster Research Center (WRC) for interesting them in this project. We also thank T. L. Bluhm of Xerox Research Centre of Canada (XRCC) for the x-ray diffraction measurements, C. Kuo of XRCC for the bulk density measurements, and E. N. Dalal and S. Blaszak of WRC for the spectra of the toner film samples.

*Present address (corresponding author), Centre de Recherches en Physique du Solide, Département de Physique, Université de Sherbrooke, Sherbrooke, Québec J1K 2R1, Canada.

REFERENCES AND NOTES

1. P. A. Lewis and T. C. Patton, eds., *The Pigment Handbook* (Wiley, New York, 1973), Vols. 1–3.
2. F. W. Billmeyer, Jr., and M. Saltzman, *Principles of Color Technology*, 2nd ed. (Wiley, New York, 1981).
3. J. Fabian and H. Hartman, "Light absorption of organic colorants: theoretical treatment and empirical rules," in *Reactivity and Structure; Concepts in Organic Chemistry*, K. Hafner, J. M. Lehn, C. W. Rees, P. von Ragué-Schleyer, B. M. Trost, and R. Zahnradník, eds. (Springer-Verlag, Berlin, 1980), Vol. 12, pp. 1–19.
4. M. Gouterman, "Optical spectra and atomic structure," in *The Porphyrins*, Part 3 of Physical Chemistry A, D. Dolphin, ed. (Academic, New York, 1978), pp. 1–159.
5. F. H. Moser and A. L. Thomas, *Phthalocyanine Compounds* (Reinhold, New York, 1963), pp. 292–307.
6. M. J. Stillman and T. Nyokong, "Absorption and magnetic circular dichroism spectral properties of phthalocyanines, Part 1: Complexes of the dianion Pc(−2)," in *Phthalocyanine: Properties and Applications*, C. C. Leznoff and A. B. P. Lever, eds. (VCH Publishers, New York, 1989), pp. 133–290.
7. R. M. Johnson, "Color theory," in *The Pigment Handbook*, T. C. Patton, ed. (Wiley, New York, 1973), Vol. 3, pp. 229–288.
8. W. Carr, "Pigment powders and dispersions: measurement and interpretation of their physical properties," in *The Pigment Handbook*, T. C. Patton, ed. (Wiley, New York, 1973), Vol. 3, pp. 11–27.
9. G. Mie, "Beiträge zur Optik trüber Medien, speziell kolloidalen Metallösungen," Ann. Phys. (Leipzig) **25,** 377–445 (1908).
10. C. F. Bohren and D. R. Huffman, *Absorption and Scattering of Light by Small Particles* (Wiley, New York, 1983).
11. W. G. Egan and T. W. Hilgeman, *Optical Properties of Inhomogeneous Materials* (Academic, New York, 1979).
12. H. C. van de Hulst, *Light Scattering by Small Particles* (Dover, New York, 1981).
13. F. Wooten, *Optical Properties of Solids* (Academic, New York, 1972), pp. 173–185.
14. E. L. Pankove, *Optical Processes in Semiconductors* (Dover, New York, 1971), pp. 87–91.
15. E. E. Bell, "Optical constants and their measurement," in *Handbuch der Physik*, S. Flügge, ed. (Springer-Verlag, Heidelberg, 1967), Vol. 25, pp. 1–58.
16. L. Edwards and M. Gouterman, "Vapor absorption spectra and stability: phthalocyanines," J. Mol. Spectrosc. **33,** 292–310 (1970).
17. B. R. Hollebone and M. J. Stillman, "Assignment of absorption and magnetic circular dichroism spectra of solid, α phase metallophthalocyanines," J. Chem. Soc. Faraday Trans. 2 **74,** 2107–2127 (1978).
18. P. Day and J. P. Williams, "Spectra and photoconduction of phthalocyanine complexes (I)," J. Chem. Phys. **37,** 567–570 (1962).
19. A. J. McHugh, M. Gouterman, and C. Weiss, Jr., "Porphyrins XXIV. Energy, oscillator strength and Zeeman splitting calculations (SCMO-CI) for phthalocyanine, porphyrins and related ring systems," Theor. Chim. Acta **24,** 346–370 (1972).
20. A. M. Schaffer and M. Gouterman, "Porphyrins XXV. Extended Hückel calculations on location and spectral effects of free base protons," Theor. Chim. Acta **25,** 62–82 (1972).
21. A. M. Schaffer and M. Gouterman, "Porphyrins XXVIII. Extended Hückel calculations on metal phthalocyanines and tetraporphins," Theor. Chim. Acta **30,** 9–30 (1973).
22. K. D. Cummings, D. B. Tanner, and J. S. Miller, "Optical properties of cesium tetracyanoquinodimethanide, $Cs_2(TCNQ)_3$," Phys. Rev. B **24,** 4142–4154 (1981).
23. Note that the contribution of the numerical integral over the data to the phase spectrum (the time-consuming step) need be made only once.
24. G. L. Carr, S. Perkowitz, and D. B. Tanner, "Far-infrared properties of inhomogeneous materials," in *Infrared and Millimeter Waves*, K. J. Button, ed. (Academic, New York, 1985), Vol. 13, pp. 171–263.
25. A copy of this program may be obtained from the authors.
26. P. R. Bevington, *Data Reduction and Error Analysis for the Physical Sciences* (McGraw-Hill, New York, 1969).
27. L. Bajema, M. Gouterman, and B. Meyer, "Absorption and fluorescence spectra of matrix isolated phthalocyanines," J. Mol. Spectrosc. **27,** 225–235 (1968).
28. J. Griffiths, "Developments in chemistry and technology of organic dyes," in *Critical Reports on Applied Chemistry*, J. Griffiths, ed. (Blackwell, Oxford, 1984), Vol. 7, p. 2.
29. J. R. Platt, "Classification and assignments of ultraviolet spectra of conjugated organic molecules," J. Opt. Soc. Am. **43,** 252–257 (1953).
30. See, for example, Ref. 2, p. 102, and Ref. 7, p. 247.
31. Z. Zhang, M. M. Lerner, V. J. Marty, and P. R. Watson, "Scanning tunneling microscopy on pressed powders," Langmuir **8,** 369–371 (1992).